Mucolipin controls lysosome exocytosis in Dictyostelium

Lima, Wanessa Cristina; Leuba, Florence; Soldati, Thierry; Cosson, Pierre

How to cite

LIMA, Wanessa Cristina et al. Mucolipin controls lysosome exocytosis in Dictyostelium. In: Journal of cell science, 2012, vol. 125, n° 9, p. 2315–2322. doi: 10.1242/jcs.100362

This publication URL: https://archive-ouverte.unige.ch/unige:18871
Publication DOI: 10.1242/jcs.100362

JCS ePress online publication date 22 February 2012

Mucolipin controls lysosome exocytosis in *Dictyostelium*

Wanessa C. Lima *[1], Florence Leuba [2], Thierry Soldati [2], Pierre Cosson [1]

[1] Dept. of Cell Physiology and Metabolism, Faculty of Medicine, University of Geneva, 1211 Geneva, Switzerland.

[2] Dept. of Biochemistry, Faculty of Sciences, University of Geneva, 1211 Geneva, Switzerland.

* Corresponding author:

Wanessa C. Lima

Dept. of Cell Physiology and Metabolism, Centre Medical Universitaire, University of Geneva,

1 rue Michel Servet, 1211 Geneva 4, Switzerland

Phone: +41223795294, Fax: +41223795260

Email: Wanessa.DeLima@unige.ch

Running title: Mucolipin controls lysosome exocytosis

Keywords: mucolipin, secretory lysosomes, mucolipidosis type IV, calcium, lysosome exocytosis

SUMMARY

Mucolipidosis type IV is a still poorly understood lysosomal storage disease caused by alterations in the mucolipin lysosomal calcium channel. In this study, we generated *mucolipin* knockout *Dictyostelium* cells, and observed that lysosome exocytosis was markedly increased in these cells compared to wild-type cells. In addition, *mucolipin* KO cells were more resistant to calcium deprivation, and the calcium concentration in their secretory lysosomes was decreased, suggesting that mucolipin transfers calcium ions from the cytosol to the lumen of secretory lysosomes. We speculate that mucolipin attenuates the fusogenic effect of local cytosolic calcium increases by dissipating them into the lumen of lysosomal compartments.

INTRODUCTION

In eukaryotic cells, endocytosed material is transported through early and late endosomes, and eventually reaches lysosomes, where it is degraded. In addition, in some specialized cells lysosomes can fuse with the cell surface in a regulated manner. Exocytosis of secretory lysosomes notably plays an important role in the biology of melanocytes or cytotoxic T-cells (Blott and Griffiths, 2002). Fusion of lysosomes with the cell surface can be triggered by transient increases in the cytosolic free calcium concentration, from the resting 0.1 μM concentration to 1-5 μM (Rodriguez et al., 1997; Andrews, 2000), and this fusion is potentially regulated by calcium transporters present at the lysosomal membrane.

Mucolipidosis type IV is a neurodegenerative lysosomal storage disorder (Berman et al., 1974), characterized by abnormally large lysosomes containing electron-dense inclusions and lipid storage bodies (Folkerth et al., 1995). It is caused by mutations in the *MCOLN1* gene (Bargal et al., 2000; Bassi et al., 2000; Sun et al., 2000), which encodes a transient receptor potential (TRP) channel, named mucolipin-1 (or TRP-ML1). Mucolipin-1 is a putative calcium channel (Raychowdhury et al., 2004) localized in the membrane of late endosomes and lysosomes (Manzoni et al., 2004; Pryor et al., 2006). Mammalian cells can also express two other endosomal mucolipin paralogs (TRP-ML2 and 3) (Cheng et al., 2010).

The role of mucolipin in lysosomal biogenesis and/or function is still poorly understood. It has been proposed that loss of mucolipin may affect either lysosomal acidification or intracellular transport. An altered lysosomal pH could affect lysosomal enzyme activity and cargo degradation and thus

account for the accumulation of undigested material in lysosomes (Bach et al., 1999; Soyombo et al., 2006). However, some studies concluded that lysosomal pH was decreased in knockout cells (Miedel et al., 2008), others reported an increased lysosomal pH (Bach et al., 1999; Soyombo et al., 2006) and others yet an unchanged lysosomal acidification (Pryor et al., 2006). Other studies have suggested that loss of TRP-ML1 may alter intracellular transport, in particular lysosome biogenesis (Tellez-Nagel et al., 1976; Treusch et al., 2004; Martina et al., 2009) and lysosome exocytosis (LaPlante et al., 2006). TRP-ML2 and TRP-ML3 are also thought to play a role in the physiology of the endocytic pathway, although their exact function remains to be established (Cheng et al., 2010)

The amoeba *Dictyostelium discoideum* is a model organism widely used to study the endocytic pathway. In these cells, endocytosed material is first transported to acidic lysosomes, and subsequently transferred to less acidic compartments, the post-lysosomes (PLs) (Maniak, 2003). PLs are functionally equivalent to mammalian secretory fusion-competent lysosomes, and they are constitutively exocytosed, releasing undigested material in the extracellular medium (Charette and Cosson, 2007). Like lysosomes, *Dictyostelium* PLs contain a putative copper transporter (referred to as p80) but unlike lysosomes, they are devoid of vacuolar H^+-ATPase. Thus, unlike mammalian secretory lysosomes, they can be formally distinguished from other lysosomes, a key advantage for studying their biogenesis and exocytosis (Charette and Cosson, 2007). Consequently, this model organism has been used previously to characterize the function of proteins involved in the biogenesis and function of secretory lysosomes, such as the orthologs of CHS and AP-3 (defective in human Chediak-Higashi and Hermanski-Pudlak syndromes, respectively) and WASH proteins (Charette and Cosson, 2007; Charette and Cosson, 2008; Carnell et al., 2011).

In this study we analyzed the phenotype of *Dictyostelium* mucolipin (*mcln*) KO cells. We expected secretory PLs to function as calcium stores releasing calcium in the cytosol through the mucolipin channel. On the contrary, our results suggest that mucolipin allows transfer of calcium from the cytosol to the lumen of PLs, thus limiting fusion of PLs with the cell surface.

RESULTS

TRP-ML localizes to secretory post-lysosomes

The *Dictyostelium* genome contains only four genes encoding putative Ca^{2+} channels (*mcln*, *pkd2*, *tpc2* and *iplA*) (Wilczynska et al., 2005). *Dictyostelium* mucolipin (Fig. 1A) exhibits the hallmarks of the TRP (transient receptor potential) family of ion channels (Venkatachalam and Montell, 2007): six transmembrane (TM) domains, a conserved pore region (position 498-511), and a characteristic large extracellular loop between TM1 and TM2 (Fig. 1B). It shares 55% of similarity with the human orthologs (TRP-ML1, 2 and 3) over the TRP similarity region (TM3 to TM6; pos. 385-541, Fig. 1C). In addition, the C-terminal cytosolic domain of *Dictyostelium* mucolipin contains a Ca^{2+}-binding EF-hand (pos. 614-626), a feature not found in other TRP-ML channels. An EF-hand is present in the C-terminal portion of the TRP-A1 channel, and accounts for the calcium-dependent activation of this channel (Doerner et al., 2007).

As observed in mammals, *Drosophila* and *C. elegans*, it is likely that *Dictyostelium* mucolipin is localized in the endosomal pathway. To assess this, an expression plasmid encoding a FLAG-tagged mucolipin was transfected into wild-type (WT) cells, which were stained with an antibody against the p80 protein. The p80 protein is an endosomal marker present in all endosomal compartments, but enriched in the secretory post-lysosomes (Ravanel et al., 2001). TRP-ML was detected in large p80-rich compartments typical of PLs, as well as in dot-like structures throughout the cytoplasm (Fig. 2A), which may also correspond to endocytic compartments (Charette et al., 2006). To confirm the endosomal localization of the FLAG-tagged mucolipin, latex-beads containing-phagosomes at different stages of maturation were purified and the presence of p80 and of FLAG-tagged mucolipin assessed (Fig. 2B). Mucolipin was faintly detected in early phagosomes, but accumulated in later phagosomes, a profile similar to that of the p80 endosomal marker (Lelong et al., 2011). Together these results indicate that mucolipin is largely present in post-lysosomes in *Dictyostelium* cells.

Endosomal pH is unaffected in *mcln* KO cells

In order to evaluate the role of mucolipin in the endocytic pathway of *Dictyostelium*, we generated *mcln* KO cells by homologous recombination (Fig. S1), and examined several key features of the endocytic pathway in these cells. Lysosomes and post-lysosomes can be identified by immunofluorescence based on the presence of two well-characterized markers, the p80 protein and vacuolar H^+-ATPase (Ravanel et al., 2001). The numbers and sizes of lysosomes (p80-positive, H^+-

ATPase-positive) and PLs (p80-positive, H^+-ATPase-negative) were indistinguishable in WT and *mcln* KO cells (Fig. S2A,B). Phagocytosis of fluorescent particles and endocytosis of fluid phase were identical in WT and mutant cells (Fig. S2D,E). Moreover, lysosomal enzymes were normally retained inside *mcln* KO cells, and secreted upon starvation (data not shown); KO cells were also able to grow normally on a large array of bacteria and to engage into multicellular development upon starvation (Fig. S3).

We studied with particular attention the pH of endosomal compartments, since conflicting results have been reported in mammalian cells. In *Dictyostelium*, endosomal pH can be measured by flow cytometry after endocytosis of a mixture of pH-sensitive and pH-insensitive fluorescent dyes (Marchetti et al., 2009) (Fig. S4). In WT cells, fluid phase is found first in very acidic lysosomes, then after 30 minutes of chase it is gradually transferred to less acidic PLs (Fig. 3A). Identical curves were obtained in *mcln* KO cells (Fig. 3A), indicating that the pH in lysosomal compartments was unaffected by mucolipin disruption. Since this technique measures an average fluorescence value over whole individual cells, it only provides an underestimated value of the pH in post-lysosomal compartments. To circumvent this limitation, we also measured directly the pH of PLs in cells loaded with fluorescent dextrans and chased for 30 minutes. PLs can easily be identified because they are large compartments where endocytosed fluid-phase is markedly concentrated (Neuhaus et al., 2002) (Fig. S4D). The post-lysosomal pH was determined directly by measuring the specific extinction of the pH-sensitive fluorescence in these compartments, and was found to be 5.6 in both WT and *mcln* KO cells (Fig. 3B). Thus, in *Dictyostelium* cells, loss of mucolipin did not result in any detectable change of endosomal pH.

PL exocytosis is dysregulated in *mcln* KO cells

Since PLs are rich in p80, their fusion with the plasma membrane leads to the transient formation of p80-rich microdomains at the cell surface, referred to as exocytic patches (Fig. 4A) (Charette and Cosson, 2007). In *mcln* KO cells, there were approximately two times more exocytic patches than in WT cells (Fig. 4B), and this phenotype was complemented when cells were transfected with an expression plasmid containing the FLAG-tagged mucolipin (Fig. 4C). Since the number of PLs per cell was the same in WT and KO cells, this suggested that the rate of fusion of individual PLs with the cell surface was two times higher in *mcln* KO cells than in WT cells (Fig. S2C). To evaluate directly and with a different method the frequency with which PLs fused with the cell surface, we fed cells with medium containing fluorescent dextran, incubated them for 30 minutes to allow transfer of endocytosed dextrans to PLs, and observed the disappearance of labeled PLs from

individual cells (Fig. 4D). These observations also indicated that the rate of fusion of individual PLs with the cell surface was significantly higher in *mcln* KO cells than in WT cells (Fig. 4E).

Transfer of phagocytosed material along the endocytic pathway can be assessed by following the maturation of endocytic compartments containing internalized fluorescent particles. In WT cells, particles are virtually all present in lysosomes for the first 30 minutes following their ingestion and then gradually transferred to PLs, where they are most prominently found after 90 minutes (Fig. 5A). In *mcln* KO cells, the majority of particles followed a similar path, being first found in lysosomes then transferred with normal kinetics to PLs. However, in addition, a significantly higher number of ingested particles was found in PLs 15 or 30 minutes after ingestion (Fig. 5B), suggesting an aberrant maturation of lysosomes into PLs. A faster biogenesis of PLs may explain why in *mcln* KO cells the faster fusion of PLs with the cell surface does not result in a decreased number of PLs when compared to WT cells.

Calcium homeostasis is affected in *mcln* KO cells

To determine if mucolipin participates in calcium homeostasis, we assessed the ability of cells to grow in calcium-depleted medium (buffered to 1 μM $CaCl_2$). In HL5 medium, WT cells reached a density of 10^6 cells/ml in 3-4 days, while in calcium-depleted medium 7-8 days were needed (Fig. 6A). Knockout *mcln* cells grew at the same rate as WT cells in HL5 medium, but in calcium-depleted medium, they grew two times faster than WT cells (Fig. 6A), suggesting that mucolipin activity in WT cells leads to a net loss of calcium from the cells.

We also assessed directly the calcium concentration in PLs in WT and *mcln* KO cells, by measuring the ratio between two dextran-coupled fluorophores, one calcium-insensitive and one calcium-sensitive. Measuring calcium concentration in lysosomes was not feasible, since the calcium probes were fully quenched by the very acidic pH in these compartments. These experiments were performed with probes binding calcium either with a high (Kd=0.6 μM) or a low (Kd=3 μM) affinity. With both probes the measured fluorescence ratio was significantly lower in PLs from *mcln* KO cells, indicating that the calcium concentration in PLs was lower in *mcln* KO cells than in WT cells (Fig. 6B). To extrapolate calcium concentrations from the fluorescence signals, the minimal and the maximal signals were determined in the presence of ionomycin and either EGTA or $CaCl_2$, respectively. In WT cells, the high-affinity probe emitted a signal identical to the maximal signal, indicating a calcium concentration higher than 1-2 μM (Fig. 6C). Accordingly, the calcium concentration was in the range covered by the low-affinity calcium probe, at approximately 3 μM

(Fig. 6D). In *mcln* KO cells both the low- and the high-affinity probes were at their minimal emission values, indicating a luminal calcium concentration lower than 0.2 μM (Fig. 6C,D).

DISCUSSION

In this study we characterized *mcln* KO cells to determine the role of the mucolipin channel in lysosome biology in *Dictyostelium*. Remarkably, the overall structure and function of the endosomal pathway was mostly unaffected in *mcln* KO cells. The pH of endosomal compartments was notably unchanged by the loss of the mucolipin protein. The only noticeable difference was that a fraction of internalized latex beads were found abnormally early in late compartments (PLs), suggesting that PLs were generated at an increased rate in *mcln* KO cells compared to WT cells. We did however observe specific alterations affecting the exocytosis of secretory lysosomes, which are discussed below.

Firstly, we observed that fusion of PLs with the cell surface was increased in *mcln* KO cells compared to WT cells. Secondly, *mcln* KO cells grew faster than WT cells in calcium-depleted medium, indicating that mucolipin plays a critical role in calcium homeostasis in these conditions. Thirdly, the calcium concentration inside PLs was around 3 μM in WT cells, and much lower (below 0.2 μM) in *mcln* KO cells. This converging series of results highlights the role of mucolipin in calcium homeostasis, and lead us to hypothesize that mucolipin actually transfers calcium from the cytosol to the PLs, and in doing so reduces the fusion of PLs with the cellular membrane (and the maturation of lysosomal compartments).

How can calcium be transferred by a mucolipin channel from the normally calcium-depleted environment of the cytosol to an intracellular compartment? To account for our observations, we speculate that PLs sometimes encounter transiently high concentrations of cytosolic calcium. Indeed, high local calcium concentrations (at least 10 μM) have been observed transiently in the vicinity of the plasma membrane in mammalian cells (Llinas et al., 1992; Marsault et al., 1997). To our knowledge, local transient calcium increases have not been studied in vegetative *Dictyostelium* cells. In developing cells, external stimuli such as cAMP or folate do cause a global cytosolic calcium increase, but the intensity of local calcium increases remains to be established (Schlatterer et al., 1994; Wilczynska et al., 2005). When such local calcium waves encounter a PL, the mucolipin channel may allow transfer of calcium inside the PLs, a mechanism similar to the efficient transfer of calcium from the endoplasmic reticulum to neighboring mitochondria (Rizzuto

et al., 1993). In that perspective it may be highly significant that the *Dictyostelium* mucolipin exhibits a cytosolic EF-hand, which may allow it to open only when the local cytosolic calcium is high. This scenario could also account for the unexpected observation that loss of mucolipin increases the fusion of PLs with the cell surface: by turning PLs into calcium sinks, mucolipin activity may decrease high local cytosolic calcium concentrations in the vicinity of PLs, thus limiting their fusion with the cell surface. This speculative model is depicted in Fig. 7. Although the simplest interpretation of our results proposes that mucolipin itself acts as a calcium channel, we however cannot exclude an indirect role of mucolipin in calcium transport across the PL membrane.

Although our knowledge of mucolipin function in mammalian cells is still incomplete, the phenotype observed for *Dictyostelium mcln* KO cells is more reminiscent of the phenotype of mammalian TRP-ML3 knockdown cells than to TRP-ML1 mutant cells. Indeed, although the three mammalian TRP-ML proteins have been shown to interact (Curcio-Morelli et al., 2010), they apparently play different and possibly antagonistic roles. TRP-ML1 KO cells show delayed endosomal traffic and decreased fusion of lysosomes to the cell surface (Pryor et al., 2006; Miedel et al., 2008). On the contrary, TRP-ML3 knockdown cells show enhanced degradation and traffic of endocytosed material and increased vesicle fusion compared to WT cells (Kim et al., 2009; Martina et al., 2009; Lelouvier and Puertollano, 2011). So far no simple explanation has been offered on how loss of TRP-ML3 could enhance membrane traffic. To date there is no consensus on the basic pore properties of mammalian TRP-ML proteins; although data points to inwardly rectifying currents for TRP-ML1 and TRP-ML3 channels, difficulties in measuring endogenous lysosomal currents have produced controversial results (Cheng et al., 2010). Some studies even showed outwardly rectifying currents for TRP-ML1 (Kiselyov et al., 2005). Mucolipin channels may be capable of transferring calcium ions in both directions, depending on the cellular environment in which they are inserted. Our studies suggest that *Dictyostelium* mucolipin functions in a manner analogous to TRP-ML3, and offer a possible explanation of how loss of a calcium channel could enhance membrane traffic.

MATERIALS AND METHODS

Cell culture and plasmids

Dictyostelium cells were grown at 21°C in HL5 medium (Cornillon et al., 2000) and subcultured twice a week to maintain a maximal density of 10^6 cells/ml. In experiments with calcium ($CaCl_2$) addition, cells were kept in HL5-MES (3.6 mM KH_2PO_4 replaced with 6.1 mM MES). For

experiments with imposed calcium concentrations, we used $CaCl_2$ and EGTA proportions defined by using the Ca-EGTA calculator program (Patton et al., 2004).

A knockout vector for *mcln* disruption was constructed using a blasticidin-resistance cassette flanked by two gene segments (positions 176-990 and 1771-2217 in the coding sequence; Fig. S1A). The PvuI-digested plasmid was introduced into DH1-10 (WT) cells (Cornillon et al., 2000) by electroporation, transfected cells were selected in the presence of blasticidin (10 μg/ml), and individual clones were screened by PCR (Fig. S1C). Three independent KO clones were used in parallel in this study, and presented identical phenotypes.

An expression vector carrying a tagged version of the mucolipin gene was constructed by introducing a C-terminal FLAG (DYKDDDDK) tagged mucolipin cDNA into pDXA-3C (Manstein et al., 1995). This plasmid was transfected into WT and *mcln* KO cells by electroporation; transfected cells were selected in the presence of G418 (10 μg/ml).

Mouse monoclonal antibodies against p80 (H161) and vacuolar H^+-ATPase (221-35-2) were described previously (Neuhaus et al., 1998; Ravanel et al., 2001). Mouse monoclonal anti-FLAG antibody (clone M2) was from Sigma-Aldrich. All fluorescent probes were from Molecular Probes, Invitrogen (Eugene, OR).

Phagosome purification and protein identification by SDS–PAGE

Phagosomes at different stages of maturation containing latex beads were purified as described (Gotthardt et al., 2006). Briefly, *Dictyostelium* cells were incubated with 0.8 μm latex beads during a pulse of 5 or 15 min, then washed and chased further for 15, 45, 105 and 165 min. Phagosomes containing latex beads were then purified by flotation on sucrose gradient. Samples of 20 μg of phagosomal proteins or 10^6 *Dictyostelium* cells were separated in 10% polyacrylamide gel, transferred to nitrocellulose membranes, and detected with primary mouse anti-FLAG and anti-p80 antibodies and secondary horseradish-peroxidase-coupled anti-mouse IgG (Bio-Rad), and revealed by chemiluminescence.

Internalization and pH measurement

The internalization of fluid phase or phagocytic particles was measured as follows: 10^6 cells were incubated at 21°C in HL5 medium containing 10 μg/ml Alexa 647-dextran (Molecular Probes, Eugene, OR) or 1 μl/ml of FITC-fluorescent 1μm diameter latex beads (Polysciences Inc., Warrington, PA) and aliquots of 10^5 cells were harvested at 30min interval up to 180min, washed

with ice-cold HL5 containing 0.1% (w/v) sodium azide, and analyzed by flow cytometry (FACS Calibur, Beckton Dickinson, San Jose, CA).

Endosomal pH was measured by flow cytometry as described previously (Marchetti et al., 2009). Briefly, *Dictyostelium* cells were incubated for 20 min in presence of two fluorescent probes: Oregon green- (pH-sensitive) and Alexa 647-dextran (pH-insensitive probe), and the fluorescence ratio of these two dyes (measured using a FACS Calibur, Beckton Dickinson, San Jose, CA) was compared to a standard calibration curve (Fig. S4C)

Fluorescence microscopy

To perform immunofluorescence, 10^6 cells were incubated on a glass coverslip for 3h at 21°C, fixed in paraformaldehyde, permeabilized with Triton X100 (0.1%) and labeled as already described (Charette and Cosson, 2006). Cells were visualized with an LSM510 confocal microscope (Carl Zeiss). The quantification of the number and diameter of lysosomes and PLs, kinetics of lysosome-PL maturation, and number of exocytic p80 patches was carried out as already described (Charette and Cosson, 2007).

To visualize PL exocytosis, 10^6 cells were incubated with 10 µg/ml Alexa 647-dextran for 3h at 21°C, washed in HL5 and allowed to attach on a glass coverslip for 30 min. Every 10 seconds, five pictures in successive focal planes separated by 2 µm were taken, using a LSM510 confocal microscope (Carl Zeiss) (total recording time: 200 seconds); for image analysis, all confocal planes were merged into a single image. PLs were identified as large endosomal compartments, where fluid phase was concentrated (see Fig. 4C); the percentage of PLs disappearing each minute was determined. At least 20-30 cells were analyzed for each cell line in each experiment.

To measure directly post-lysosomal pH, 10^6 cells were incubated in HL5 containing 10 µg/ml Alexa 647- (pH-insensitive) and 25 µg/ml of FITC-dextran (pH-sensitive) for 3h at 21°C, washed in HL5 and allowed to attach to a glass coverslip for 30 min. Pictures of live cells were taken with an LSM510 confocal microscope (Carl Zeiss), and at least 100 PLs were analyzed for each condition tested (see Fig. S4D). The fluorescence ratio was calculated and compared to a standard calibration curve (obtained by buffering cells with 40 mM NH_4Cl + 0.1% (w/v) sodium azide at pH 4 to 7, Fig. S4E).

Calcium probes are too sensitive to acidic pH to assess calcium concentration in very acidic lysosomes, but adequate in the more neutral PLs. To measure post-lysosomal calcium levels, 10^6

cells were incubated with 10 µg/ml Alexa 647- (calcium-insensitive) and 50 µg/ml Fluo4-dextran (calcium-sensitive, either in its high affinity form, Kd=0.6 µM or low affinity, Kd=3 µM) for 3h at 21°C, washed in HL5 and allowed to attach to a glass coverslip for 30 min. Pictures were taken with a LSM510 confocal microscope (Carl Zeiss), and at least 100 PLs were counted for each condition. The fluorescence ratio (R) was calculated, and compared to the minimal (R_{min}) and maximal (R_{max}) ratios, measured after incubating cells for 15 min in presence of 20 µM ionomycin and 20 mM EGTA or $CaCl_2$, respectively. The calcium concentration was estimated when appropriate by using the formula $[Ca] = Kd * (R-R_{min}) / (R_{max} - R)$.

Sequence and phylogenetic analysis

Sequence similarity analyses were performed using BlastP and tBlastN programs against the nucleotidic or proteic databases deposited at NCBI or DictyBase servers (Pruitt et al., 2005; Chisholm et al., 2006). For phylogenetic analyses, protein sequences were aligned by using CLUSTALX 2.0 program (Larkin et al., 2007). Pair-wise genetic distances were computed by using MEGA 4.0 (Tamura et al., 2007), with the JTT (Jones–Taylor–Thornton) model of amino acid replacement, gamma-distributed rate (4 categories) and inferred alpha-parameter. Maximum likelihood (ML) trees were set up with RAxML 7.0.4 (Stamatakis, 2006), with the WAG model, and parameters for invariable sites and gamma-distributed rate heterogeneity (4 categories). One thousand bootstrap replicates were executed and bootstrap values drawn up on the best-scoring ML-tree. Trees were visualized using MEGA 4.0.

Statistical analysis

Unless otherwise specified, for quantified data, the average and s.e.m. of at least three independent experiments are indicated. Statistical comparisons were done with student t-tests (two-tailed, paired); *: $p<0.05$; **: $p<0.01$.

ACKNOWLEDGEMENTS

The P.C. and T.S. laboratories are supported by the Swiss National Foundation for Scientific Research (grants 31003A-135789 and 31003A_132995, respectively), the Doerenkamp-Zbinden Foundation, and the E. Naef Foundation (FENRIV). We thank Pierre Golstein, Nicolas Demaurex and Oliver Hartley for critical reading of this manuscript.

REFERENCES

Andrews, N. W. (2000). Regulated secretion of conventional lysosomes. *Trends Cell Biol* **10**, 316-321.

Bach, G., Chen, C. S. and Pagano, R. E. (1999). Elevated lysosomal pH in Mucolipidosis type IV cells. *Clin Chim Acta* **280**, 173-179.

Bargal, R., Avidan, N., Ben-Asher, E., Olender, Z., Zeigler, M., Frumkin, A., Raas-Rothschild, A., Glusman, G., Lancet, D. and Bach, G. (2000). Identification of the gene causing mucolipidosis type IV. *Nat Genet* **26**, 118-123.

Bassi, M. T., Manzoni, M., Monti, E., Pizzo, M. T., Ballabio, A. and Borsani, G. (2000). Cloning of the gene encoding a novel integral membrane protein, mucolipidin-and identification of the two major founder mutations causing mucolipidosis type IV. *Am J Hum Genet* **67**, 1110-1120.

Berman, E. R., Livni, N., Shapira, E., Merin, S. and Levij, I. S. (1974). Congenital corneal clouding with abnormal systemic storage bodies: a new variant of mucolipidosis. *J Pediatr* **84**, 519-526.

Blott, E. J. and Griffiths, G. M. (2002). Secretory lysosomes. *Nat Rev Mol Cell Biol* **3**, 122-131.

Carnell, M., Zech, T., Calaminus, S. D., Ura, S., Hagedorn, M., Johnston, S. A., May, R. C., Soldati, T., Machesky, L. M. and Insall, R. H. (2011). Actin polymerization driven by WASH causes V-ATPase retrieval and vesicle neutralization before exocytosis. *The Journal of cell biology* **193**, 831-839.

Charette, S. J. and Cosson, P. (2006). Exocytosis of late endosomes does not directly contribute membrane to the formation of phagocytic cups or pseudopods in Dictyostelium. *FEBS Lett* **580**, 4923-4928.

Charette, S. J. and Cosson, P. (2007). A LYST/beige homolog is involved in biogenesis of Dictyostelium secretory lysosomes. *J Cell Sci* **120**, 2338-2343.

Charette, S. J. and Cosson, P. (2008). Altered composition and secretion of lysosome-derived compartments in Dictyostelium AP-3 mutant cells. *Traffic* **9**, 588-596.

Charette, S. J., Mercanti, V., Letourneur, F., Bennett, N. and Cosson, P. (2006). A role for adaptor protein-3 complex in the organization of the endocytic pathway in Dictyostelium. *Traffic* **7**, 1528-1538.

Cheng, X., Shen, D., Samie, M. and Xu, H. (2010). Mucolipins: Intracellular TRPML1-3 channels. *FEBS Lett* **584**, 2013-2021.

Chisholm, R. L., Gaudet, P., Just, E. M., Pilcher, K. E., Fey, P., Merchant, S. N. and Kibbe, W. A. (2006). dictyBase, the model organism database for Dictyostelium discoideum. *Nucleic Acids Res* **34**, D423-427.

Cornillon, S., Pech, E., Benghezal, M., Ravanel, K., Gaynor, E., Letourneur, F., Bruckert, F. and Cosson, P. (2000). Phg1p is a nine-transmembrane protein superfamily member involved in dictyostelium adhesion and phagocytosis. *J Biol Chem* **275**, 34287-34292.

Curcio-Morelli, C., Zhang, P., Venugopal, B., Charles, F. A., Browning, M. F., Cantiello, H. F. and Slaugenhaupt, S. A. (2010). Functional multimerization of mucolipin channel proteins. *J Cell Physiol* **222**, 328-335.

Doerner, J. F., Gisselmann, G., Hatt, H. and Wetzel, C. H. (2007). Transient receptor potential channel A1 is directly gated by calcium ions. *J Biol Chem* **282**, 13180-13189.

Folkerth, R. D., Alroy, J., Lomakina, I., Skutelsky, E., Raghavan, S. S. and Kolodny, E. H. (1995). Mucolipidosis IV: morphology and histochemistry of an autopsy case. *J Neuropathol Exp Neurol* **54**, 154-164.

Gotthardt, D., Blancheteau, V., Bosserhoff, A., Ruppert, T., Delorenzi, M. and Soldati, T. (2006). Proteomics fingerprinting of phagosome maturation and evidence for the role of a Galpha during uptake. *Mol Cell Proteomics* **5**, 2228-2243.

Kim, H. J., Soyombo, A. A., Tjon-Kon-Sang, S., So, I. and Muallem, S. (2009). The Ca(2+) channel TRPML3 regulates membrane trafficking and autophagy. *Traffic* **10**, 1157-1167.
Kiselyov, K., Chen, J., Rbaibi, Y., Oberdick, D., Tjon-Kon-Sang, S., Shcheynikov, N., Muallem, S. and Soyombo, A. (2005). TRP-ML1 is a lysosomal monovalent cation channel that undergoes proteolytic cleavage. *J Biol Chem* **280**, 43218-43223.
LaPlante, J. M., Sun, M., Falardeau, J., Dai, D., Brown, E. M., Slaugenhaupt, S. A. and Vassilev, P. M. (2006). Lysosomal exocytosis is impaired in mucolipidosis type IV. *Mol Genet Metab* **89**, 339-348.
Larkin, M. A., Blackshields, G., Brown, N. P., Chenna, R., McGettigan, P. A., McWilliam, H., Valentin, F., Wallace, I. M., Wilm, A., Lopez, R. et al. (2007). Clustal W and Clustal X version 2.0. *Bioinformatics* **23**, 2947-2948.
Lelong, E., Marchetti, A., Gueho, A., Lima, W. C., Sattler, N., Molmeret, M., Hagedorn, M., Soldati, T. and Cosson, P. (2011). Role of magnesium and a phagosomal P-type ATPase in intracellular bacterial killing. *Cellular microbiology* **13**, 246-258.
Lelouvier, B. and Puertollano, R. (2011). Mucolipin-3 regulates luminal calcium, acidification, and membrane fusion in the endosomal pathway. *The Journal of biological chemistry* **286**, 9826-9832.
Llinas, R., Sugimori, M. and Silver, R. B. (1992). Microdomains of high calcium concentration in a presynaptic terminal. *Science* **256**, 677-679.
Maniak, M. (2003). Fusion and fission events in the endocytic pathway of Dictyostelium. *Traffic* **4**, 1-5.
Manstein, D. J., Schuster, H. P., Morandini, P. and Hunt, D. M. (1995). Cloning vectors for the production of proteins in Dictyostelium discoideum. *Gene* **162**, 129-134.
Manzoni, M., Monti, E., Bresciani, R., Bozzato, A., Barlati, S., Bassi, M. T. and Borsani, G. (2004). Overexpression of wild-type and mutant mucolipin proteins in mammalian cells: effects on the late endocytic compartment organization. *FEBS Lett* **567**, 219-224.
Marchetti, A., Lelong, E. and Cosson, P. (2009). A measure of endosomal pH by flow cytometry in Dictyostelium. *BMC Res Notes* **2**, 7.
Marsault, R., Murgia, M., Pozzan, T. and Rizzuto, R. (1997). Domains of high Ca2+ beneath the plasma membrane of living A7r5 cells. *EMBO J* **16**, 1575-1581.
Martina, J. A., Lelouvier, B. and Puertollano, R. (2009). The calcium channel mucolipin-3 is a novel regulator of trafficking along the endosomal pathway. *Traffic* **10**, 1143-1156.
Miedel, M. T., Rbaibi, Y., Guerriero, C. J., Colletti, G., Weixel, K. M., Weisz, O. A. and Kiselyov, K. (2008). Membrane traffic and turnover in TRP-ML1-deficient cells: a revised model for mucolipidosis type IV pathogenesis. *J Exp Med* **205**, 1477-1490.
Neuhaus, E. M., Almers, W. and Soldati, T. (2002). Morphology and dynamics of the endocytic pathway in Dictyostelium discoideum. *Molecular biology of the cell* **13**, 1390-1407.
Neuhaus, E. M., Horstmann, H., Almers, W., Maniak, M. and Soldati, T. (1998). Ethane-freezing/methanol-fixation of cell monolayers: a procedure for improved preservation of structure and antigenicity for light and electron microscopies. *J Struct Biol* **121**, 326-342.
Patton, C., Thompson, S. and Epel, D. (2004). Some precautions in using chelators to buffer metals in biological solutions. *Cell Calcium* **35**, 427-431.
Pruitt, K. D., Tatusova, T. and Maglott, D. R. (2005). NCBI Reference Sequence (RefSeq): a curated non-redundant sequence database of genomes, transcripts and proteins. *Nucleic Acids Res* **33**, D501-504.
Pryor, P. R., Reimann, F., Gribble, F. M. and Luzio, J. P. (2006). Mucolipin-1 is a lysosomal membrane protein required for intracellular lactosylceramide traffic. *Traffic* **7**, 1388-1398.
Ravanel, K., de Chassey, B., Cornillon, S., Benghezal, M., Zulianello, L., Gebbie, L., Letourneur, F. and Cosson, P. (2001). Membrane sorting in the endocytic and phagocytic pathway of Dictyostelium discoideum. *Eur J Cell Biol* **80**, 754-764.
Raychowdhury, M. K., Gonzalez-Perrett, S., Montalbetti, N., Timpanaro, G. A., Chasan, B., Goldmann, W. H., Stahl, S., Cooney, A., Goldin, E. and Cantiello, H. F. (2004). Molecular

pathophysiology of mucolipidosis type IV: pH dysregulation of the mucolipin-1 cation channel. *Hum Mol Genet* **13**, 617-627.
Rizzuto, R., Brini, M., Murgia, M. and Pozzan, T. (1993). Microdomains with high Ca2+ close to IP3-sensitive channels that are sensed by neighboring mitochondria. *Science* **262**, 744-747.
Rodriguez, A., Webster, P., Ortego, J. and Andrews, N. W. (1997). Lysosomes behave as Ca2+-regulated exocytic vesicles in fibroblasts and epithelial cells. *J Cell Biol* **137**, 93-104.
Schlatterer, C., Gollnick, F., Schmidt, E., Meyer, R. and Knoll, G. (1994). Challenge with high concentrations of cyclic AMP induces transient changes in the cytosolic free calcium concentration in Dictyostelium discoideum. *J Cell Sci* **107 (Pt 8)**, 2107-2115.
Soyombo, A. A., Tjon-Kon-Sang, S., Rbaibi, Y., Bashllari, E., Bisceglia, J., Muallem, S. and Kiselyov, K. (2006). TRP-ML1 regulates lysosomal pH and acidic lysosomal lipid hydrolytic activity. *J Biol Chem* **281**, 7294-7301.
Stamatakis, A. (2006). RAxML-VI-HPC: maximum likelihood-based phylogenetic analyses with thousands of taxa and mixed models. *Bioinformatics* **22**, 2688-2690.
Sun, M., Goldin, E., Stahl, S., Falardeau, J. L., Kennedy, J. C., Acierno, J. S., Jr., Bove, C., Kaneski, C. R., Nagle, J., Bromley, M. C. et al. (2000). Mucolipidosis type IV is caused by mutations in a gene encoding a novel transient receptor potential channel. *Hum Mol Genet* **9**, 2471-2478.
Tamura, K., Dudley, J., Nei, M. and Kumar, S. (2007). MEGA4: Molecular Evolutionary Genetics Analysis (MEGA) software version 4.0. *Mol Biol Evol* **24**, 1596-1599.
Tellez-Nagel, I., Rapin, I., Iwamoto, T., Johnson, A. B., Norton, W. T. and Nitowsky, H. (1976). Mucolipidosis IV. Clinical, ultrastructural, histochemical, and chemical studies of a case, including a brain biopsy. *Arch Neurol* **33**, 828-835.
Treusch, S., Knuth, S., Slaugenhaupt, S. A., Goldin, E., Grant, B. D. and Fares, H. (2004). Caenorhabditis elegans functional orthologue of human protein h-mucolipin-1 is required for lysosome biogenesis. *Proc Natl Acad Sci U S A* **101**, 4483-4488.
Venkatachalam, K. and Montell, C. (2007). TRP channels. *Annu Rev Biochem* **76**, 387-417.
Wilczynska, Z., Happle, K., Muller-Taubenberger, A., Schlatterer, C., Malchow, D. and Fisher, P. R. (2005). Release of Ca2+ from the endoplasmic reticulum contributes to Ca2+ signaling in Dictyostelium discoideum. *Eukaryot Cell* **4**, 1513-1525.

FIGURE LEGENDS

Fig. 1: Architecture and primary structure of TRP-ML in *Dictyostelium*.

A) Unrooted maximum likelihood tree of mucolipin. Branch lengths are proportional to the number of amino acid substitutions per site. Numbers at the nodes represent the percentage of bootstrap support (upper values for the ML tree and lower values for the NJ tree. Only values > 60% are shown).

B) Schematic representation of the mucolipin channel, depicting the 6 TM domains, the pore regions, the big extracellular loop and the EF-hand domain (black box in the C-terminal region).

C) Protein alignment of the conserved TRP region, spanning TM domains 3 to 6 (boxed regions). Bold underlined residues are conserved in human (TRP-ML1, GenBank accession number NP_065394), *C. elegans* (cup-5, NP_001022722) and *Dictyostelium* (mucolipin, XP_635110) orthologs. Gaps are denoted by broken lines. The pore region is indicated by a thick line.

Fig. 2: Mucolipin localizes to endosomal compartments.

A) Confocal images of two representative FLAG-mucolipin transfected cells, labeled for the FLAG epitope (left column) and p80 protein (right column). Arrows indicate co-localization of p80-rich secretory post-lysosomes and FLAG-fused mucolipin. The smaller, p80-low compartments correspond to lysosomes (arrowheads). Scale bar: 5µm.

B) Latex-beads containing-phagosomes at different stages of maturation were purified and the presence of p80 (lower panel) and of FLAG-tagged mucolipin (upper panel) assessed by Western blot. Both mucolipin and p80 accumulated specifically in late phagosomal compartments. NT: non-transfected cells, T: FLAG-mucolipin transfected cells.

Fig. 3: Mucolipin is not involved in the control of lysosomal pH

A) Endosomal pH was determined as the fluorescence ratio of two internalized probes (pH-insensitive and pH-sensitive dextrans) at different chase times compared to a calibration curve (Fig. S4).

B) Post-lysosomal pH was determined by measuring directly the fluorescence ratio in PLs and comparing to a calibration curve (Fig. S4E).

Fig. 4: Role of mucolipin in lysosome exocytosis

A) Confocal image of a typical PL exocytic p80 patch at the cell surface (arrow).

B) The percentage of cells exhibiting an exocytic patch was determined for WT and KO cells.

C) The percentage of cells exhibiting an exocytic patch in WT and KO cells transfected with a FLAG-tagged TRP-ML expression plasmid.

D) Successive pictures of a live WT cell fed with fluorescent dextran; each image represents a merge of confocal pictures covering the whole cell. Arrows indicate one PL that disappeared after 30 sec of observation. In this cell, a new PL formed after 20 sec (arrowheads).

E) The percentage of PLs exocytosed per minute was determined.

Scale bars: 5µm.

Fig. 5: Abnormal lysosome maturation in *mcln* KO cells

A) Confocal images of internalized beads (in white, in the merge pictures) either in lysosomes (top panel: H^+-ATPase positive compartments, arrowheads) or PLs (lower panel: H^+-ATPase negative compartments, arrows). Contractive vacuole can be seen as H^+-ATPase positive, p80 negative compartments closely apposed to the plasma membrane (pinheads). Scale bar: 5µm.

B) WT or *mcln* KO cells were fed latex beads, then chased for the indicated times. The percentage of internalized beads present in PLs is indicated (all other beads were found in lysosomes).

Fig. 6: Calcium homeostasis is affected in *mcln* KO cells

A) Faster growth of *mcln* KO cells in calcium-depleted medium (1µM $CaCl_2$); this representative experiment was repeated three times with similar results.

B) Decreased calcium concentration in PLs of *mcln* KO cells. The calcium concentration in PLs was determined by measuring the fluorescence ratio of internalized calcium-sensitive and calcium-insensitive probes.

C-D) Calcium calibration for Fluo4 high- (C) and low- (D) affinity probes. Maximum and minimum values were obtained as described in the Methods section. To allow comparisons between independent experiments, the FL1/FL4 ratio values for WT cells for each fluorophore were normalized to 100%.

Fig. 7: A speculative model of the role of mucolipin in *Dictyostelium* cells

In WT cells, cytosolic calcium waves reaching a secretory post-lysosome can diffuse into the compartment lumen through the mucolipin channel. In *mcln* KO cells, disruption of the channel prevents calcium buffering, and a high local cytosolic calcium concentration persists longer in the vicinity of the PL, promoting its fusion with the plasma membrane. Grey shades and (+) signs depict calcium concentration in a figurative way.

SUPPLEMENTAL FIGURE LEGENDS

Fig. S1: Generation of *mcln* KO cells

A) Schematic representation of mucolipin gene in WT and KO cells. Arrows indicate the position of oligos (described in C) used to construct the KO vector and to screen the KO cells.

B) Schematic representation of KO vector, indicating cloning restriction sites and PvuI linearization site.

C) Sequence and position (numbers refer to position on the genomic sequence of the gene) of oligos used for cloning and screening.

D) KO cells were screened by PCR.

Fig. S2: Normal organization of the endocytic pathway in *mcln* KO cells

A) and B) Cells were processed for immunofluorescence to detect p80 and H^+-ATPase and distinguish lysosomes (Ly) and post-lysosomes (PL) (as depicted in Fig. 5A). Number of compartments per cell (A) and average compartment size (B) were assessed, and no difference was observed between WT and *mcln* KO cells.

C) PL exocytosis in WT and *mcln* KO cells. PL/cell refers to average number of PLs per cell ± SEM (n = 3) (as determined in A). Patch is the percentage of cells presenting a p80 patch (as determined in Fig. 4B). The fusion efficacy (a.u.) was calculated by dividing the frequency of p80 patches by the number of PLs.

D) and E) Cells were allowed to internalize Alexa-647 dextran or FITC-latex beads for up to 180 min (to measure endocytosis and phagocytosis, respectively) and internalized fluorescence was measured every 30 min by flow cytometry (FACS). Values for WT at time point 120 min were arbitrarily defined as 100%. No significant difference in internalization was observed between WT and *mcln* KO cells.

Fig. S3: Multicellular development and growth in bacteria are unaffected in *mcln* KO cells.

A) WT and KO cells were harvested, resuspended in phosphate buffer and plated on black nitrocellulose filters. Multicellular development was observed after 24 hs. Two representative pictures are shown. KO cells formed fruiting bodies with the same kinetics as WT cells, and they were identical in size or number. Scale bar: 1 mm.

B) 1000 *Dictyostelium* cells were applied on a bacterial lawn (black), and growth was observed after 4-7 days by the formation of a phagocytic plaque (white). For all bacteria tested, *mcln* KO cells grew like WT cells. Tested bacteria included two gram-positive (Bs: *Bacillus subtilis* and Ml:

Micrococcus luteus) and three Gram-negative (Kp: *Klebsiella pneumoniae*, Ec: *Escherichia coli*, PT531: a permissive strain of *Pseudomonas aeruginosa*).

Fig. S4: Measurement of endosomal and post-lysosomal pH

A-C) Cells were incubated 20 min in presence of Oregon green- (pH sensitive) and Alexa-647 (pH insensitive) dextran probes, washed and chased up to 120 min in HL5; intracellular fluorescence was measured by flow cytometry at each indicated time. This experiment was repeated 3 times with equivalent results. Cell-associated fluorescence of both OG- (A) and Alexa-647 (B) dextrans presents the same kinetics in WT and *mcln* KO cells, although the latter has lower absolute values (as expected by the lower levels of fluid-phase endocytosis, Fig. S2). A calibration curve (C) was obtained in parallel by imposing a range of pH (4 to 6), in the presence of sodium azide and ammonium chloride. The ratio of FL1/FL4 fluorescences is indicated for each measured pH, and these values can be used to extrapolate endosomal pH in Fig. 3A.

D) and E) Cells were incubated 3 h in presence of FITC- (pH sensitive) and Alexa-647 (pH insensitive) dextran probes, washed and chased for 30 min in HL5; post-lysosomal fluorescence was measured by confocal pictures (D shows a representative picture of a cell with two post-lysosomes). A calibration curve (E) was obtained in parallel by imposing a range of pH (5 to 7), in the presence of sodium azide and ammonium chloride. The ratio of FL1/FL4 fluorescences is indicated for each measured pH, and these values can be used to extrapolate post-lysosomal pH in Fig. 3B. This experiment was repeated 3 times with equivalent results.

Figure 1

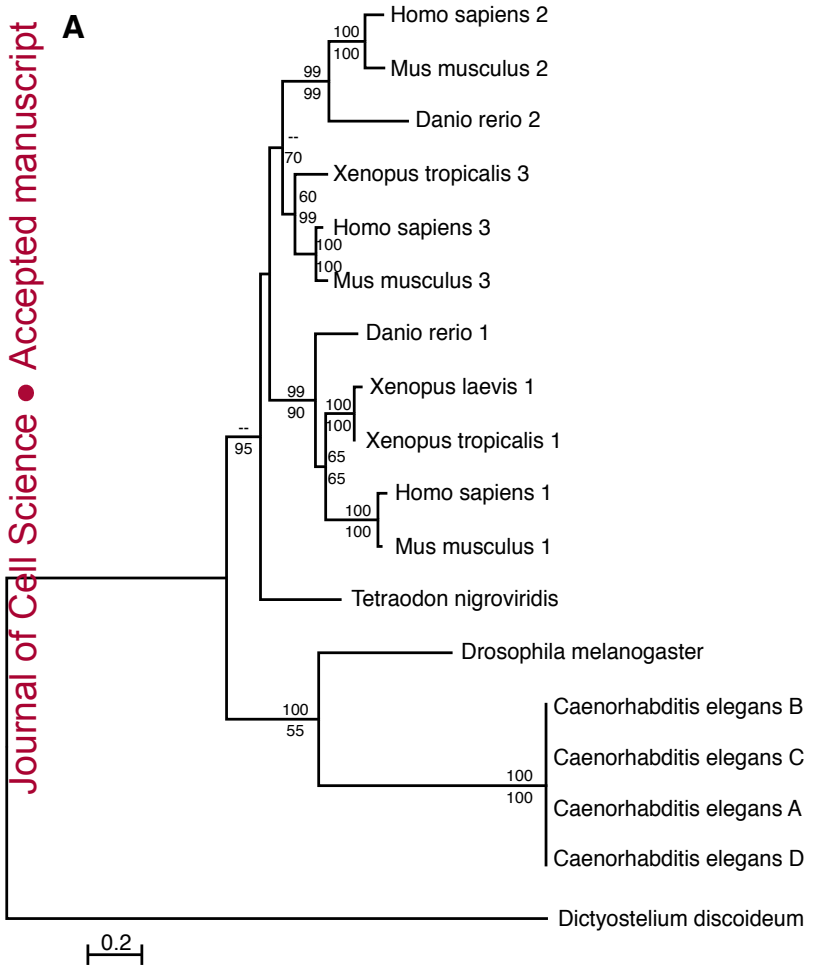

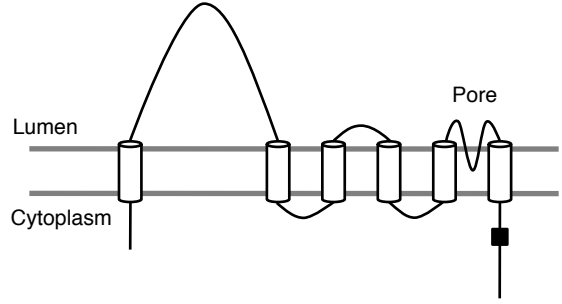

C

```
HUMAN FRLLFDVVVILTCSLSFLLCARSLLRGFLLQNEFVGFMWRQRG----
CAEEL LIGGTDIFVLILCILSLILCCRALIKAHLLQIKTSDYFENVLK----
DICDY SKLILDSFIIVLSILSQILAWRSFVFSFKTYQRTKRLLRRNSTRSLL

HUMAN ----RVISLWERLFFVNGWYILLVTSDVLTISGTIMKIGIEAKN--L
CAEEL ----NKITVTDQLDFLNLWYVMIVVNDALIIIGTVAKISIEFQDFDN
DICDY TVNWKSLSWKTKLRFFNLWFVLCLISNVLTIAGAILDFFEVPGT---

HUMAN ASYDVCSILLGTSTLLVWVGVIRYLTFFHNYNILIATLRVALPSVMR
CAEEL SLFTLTSIFLGMGALLVYVGVLRYFGFFSQYNILMLTLKRSAPNIMR
DICDY VSSTATKVLIGLGTLLSWINMIRYLEFDTKSTSLIRALINGLPEIIR

HUMAN FCCCVAVIYLGYCFCGWIVLGPYHVKFRSLSMVSECLFSLINGDDMF
CAEEL FMTCAIVLYAGFLIAGWVIIGPYSMKFRTLAESSEALFSLLNGDDMF
DICDY FSAGSLPIFIGFCLFGLMVFSEHTLRFASFGEAAITLFGLQNGDDVQ

HUMAN VTFAAMQAQQGRSSLVWLFSQLYLYSFISLFIYMVLSLFIALI
CAEEL ATFYTINDS---NTVIKVFGTVYIYLFVSLFIYVVLSLFIAII
DICDY ATFRATEKD-------PIISKMYFFVFVFISVYCISNIYIAIM
```

Figure 2

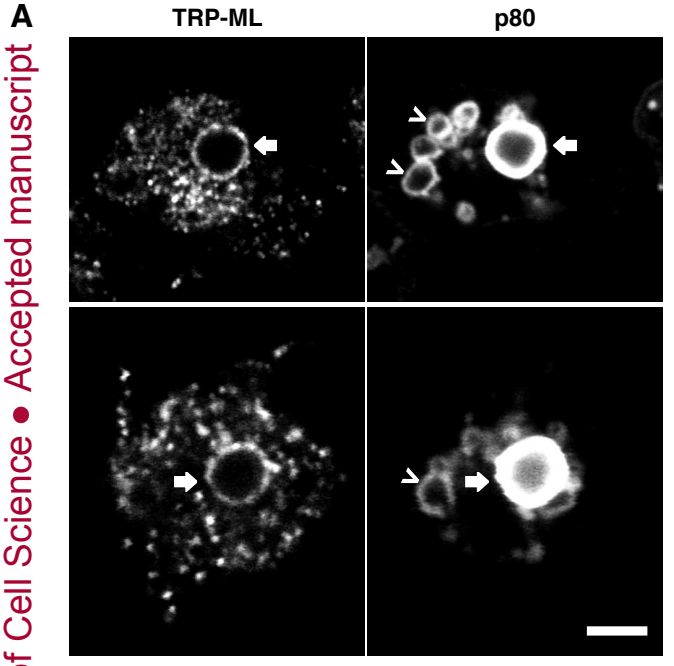

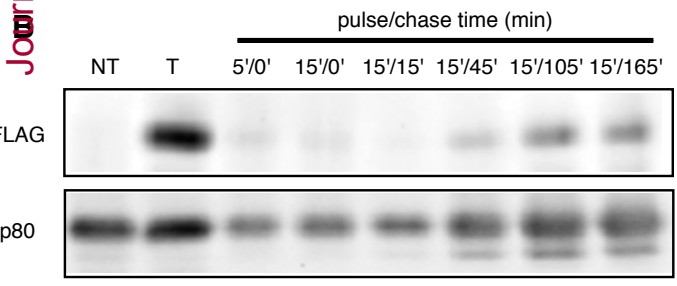

Figure 3

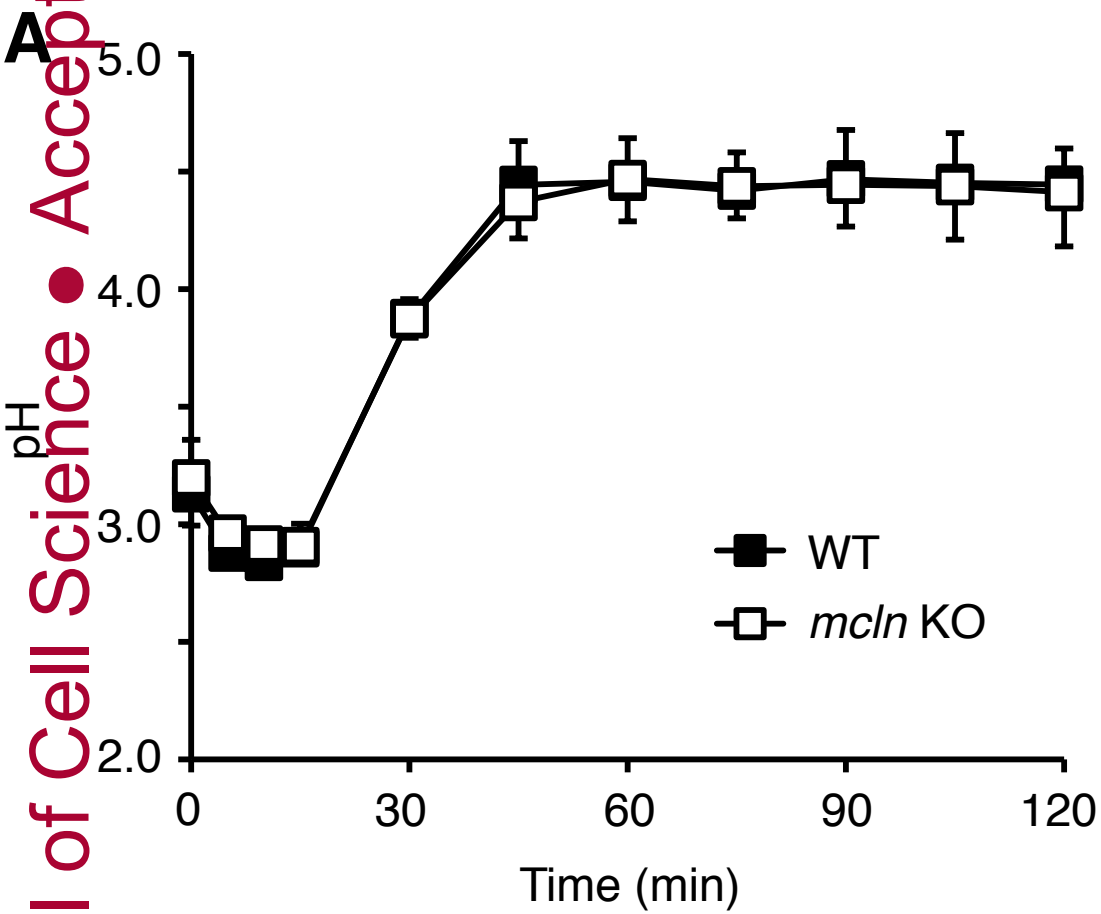

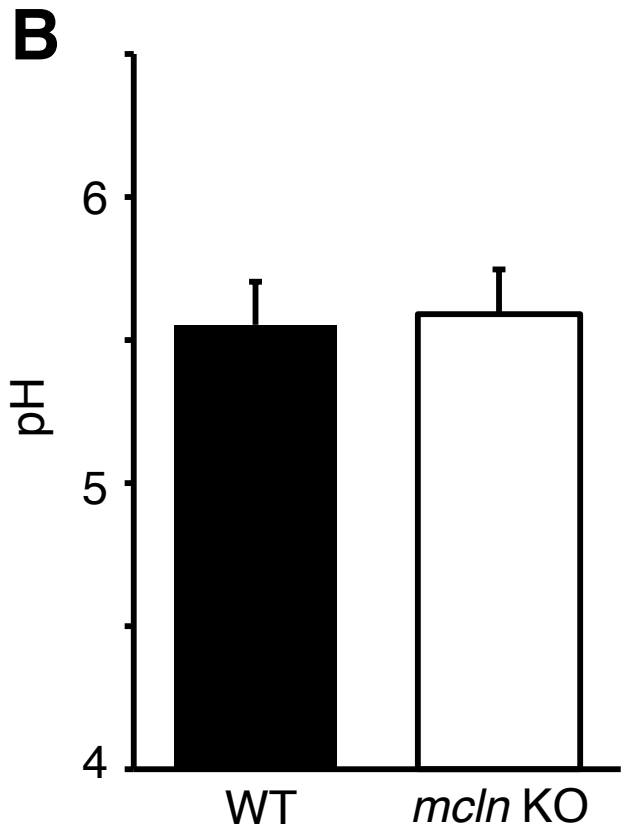

Figure 4

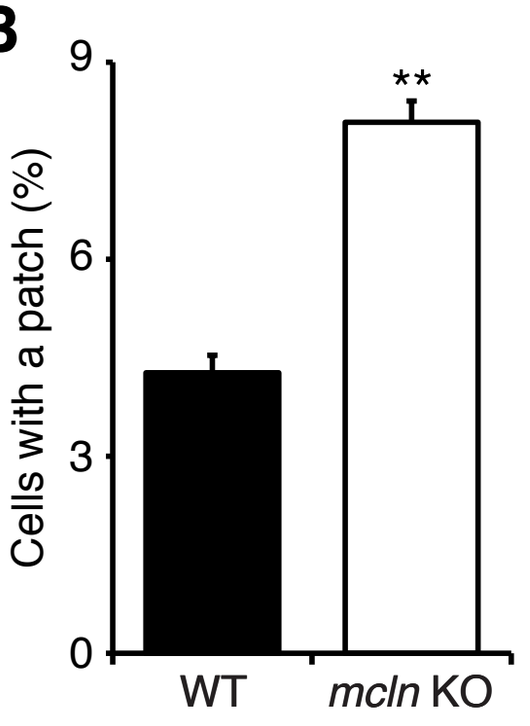

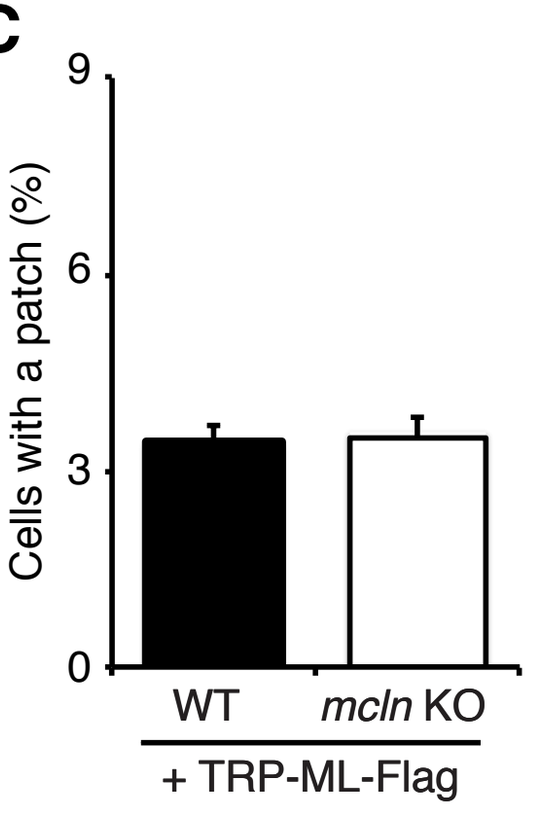

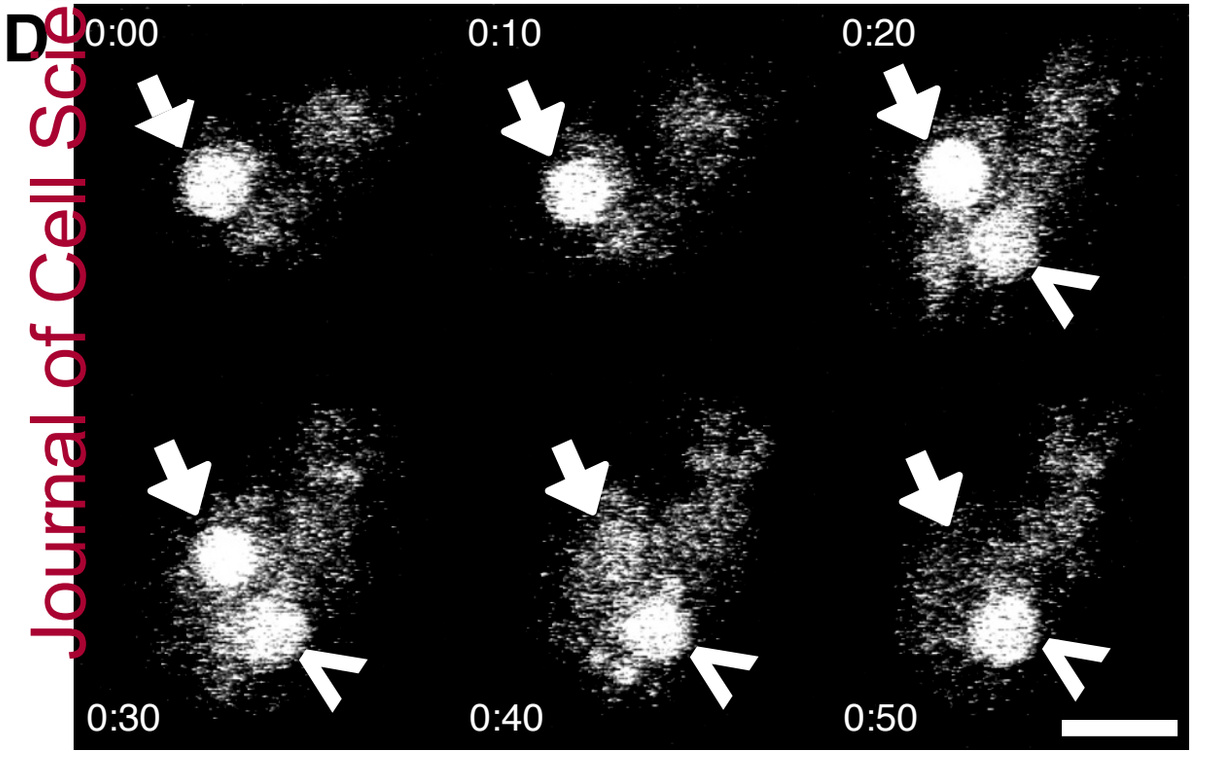

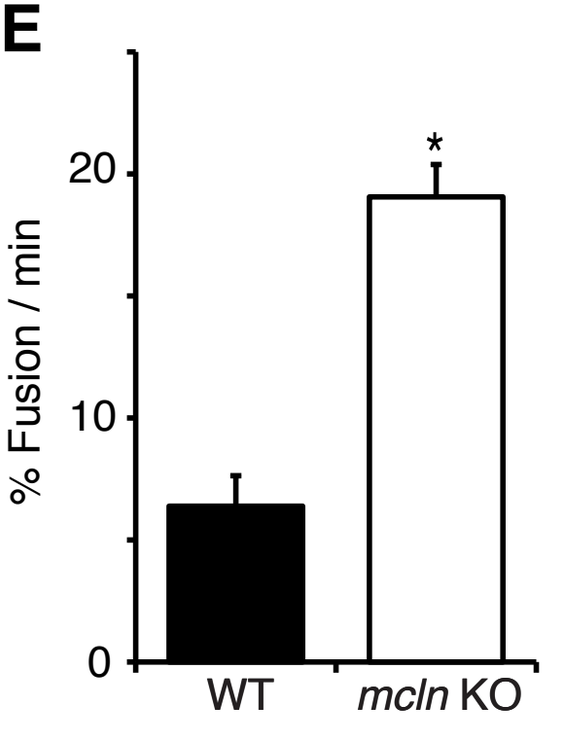

Figure 5

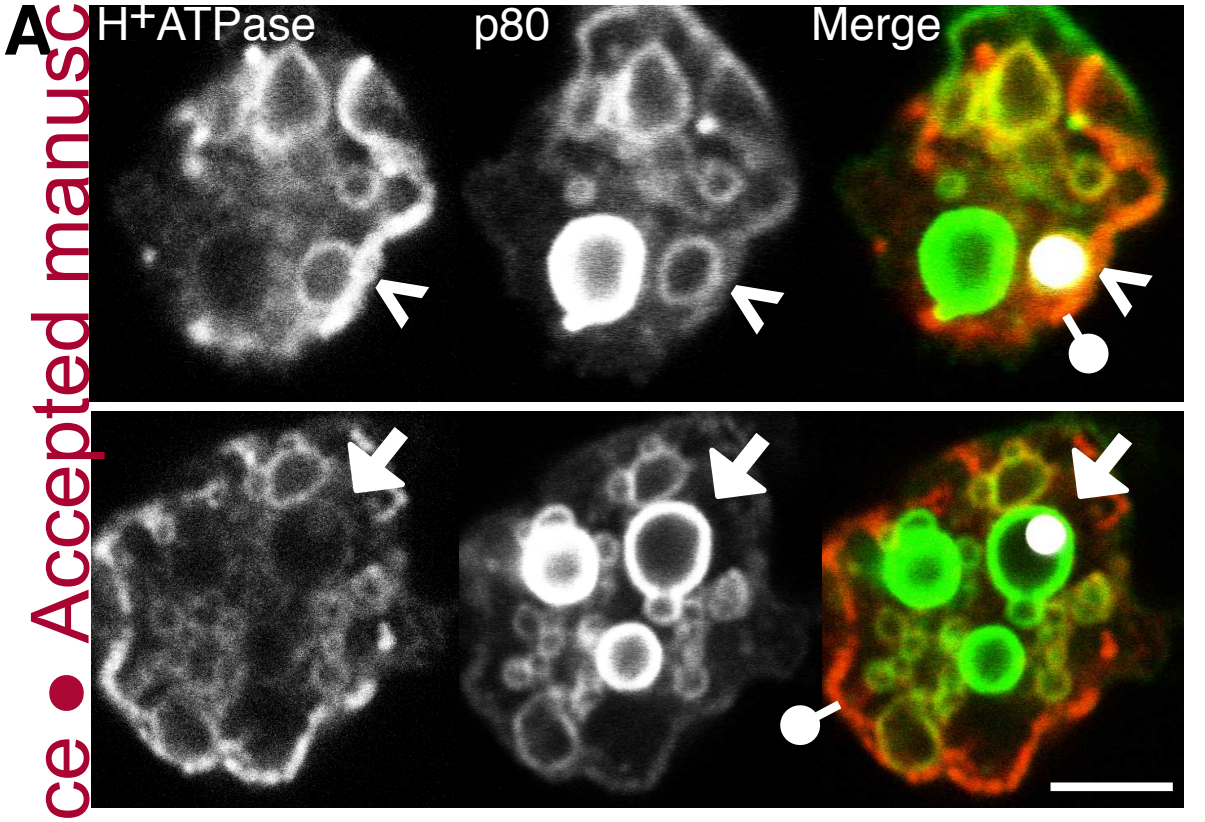

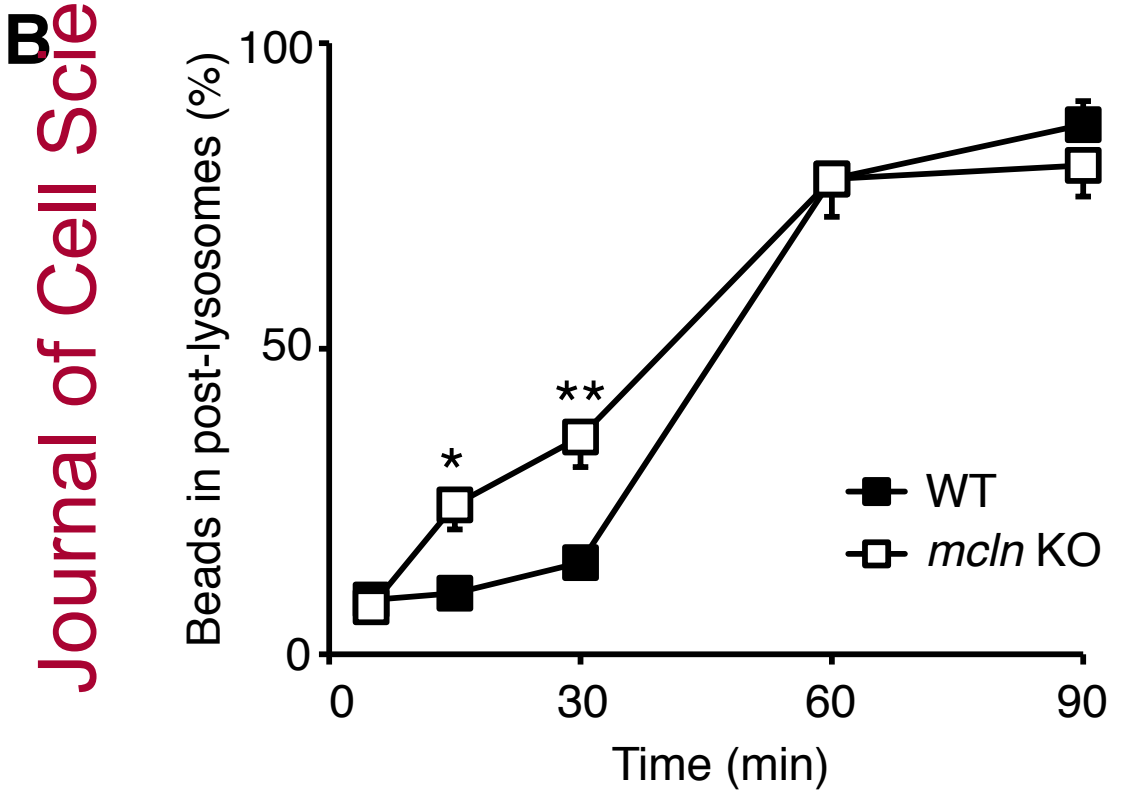

Figure 6

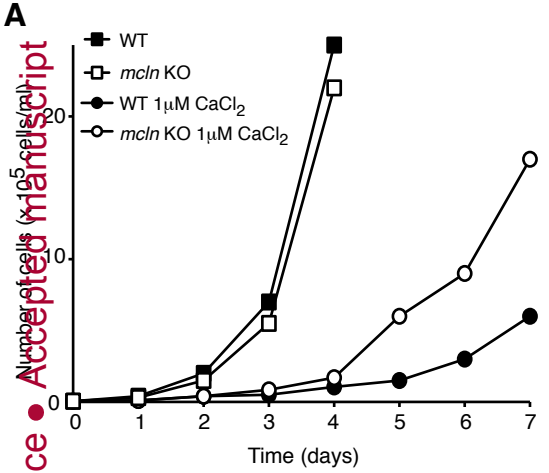

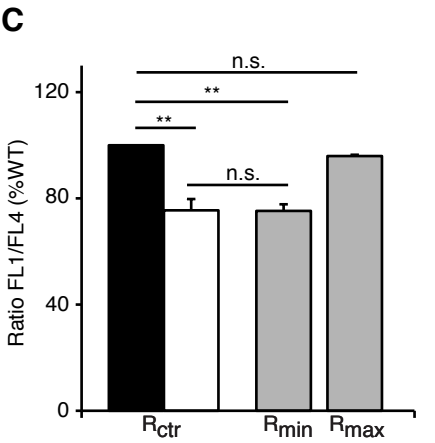

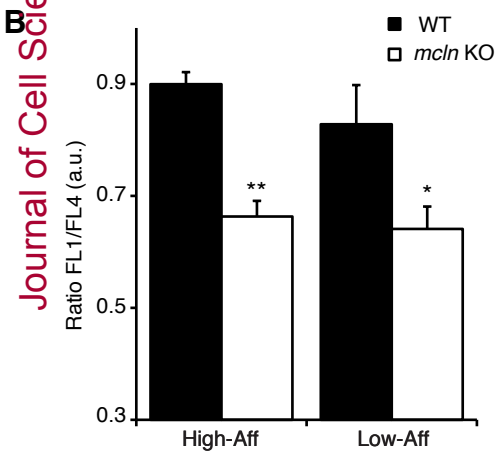

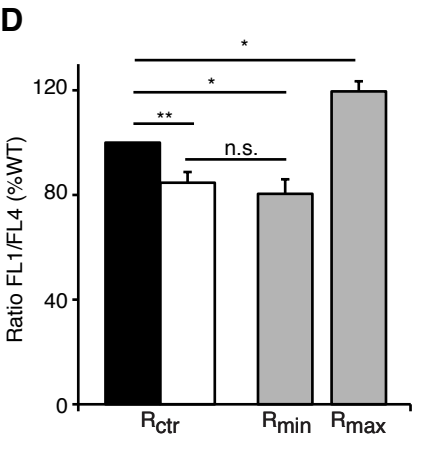

Figure 7